

OKU Fen Bilimleri Enstitüsü Dergisi 8(4): 1644-1653, 2025

OKU Journal of The Institute of Science and Technology, 8(4): 1644-1653, 2025

Osmaniye Korkut Ata Üniversitesi Fen Bilimleri Enstitüsü Dergisi

Osmaniye Korkut Ata University Journal of The Institute of Science and Technology



Influence of Intense Laser Field on the Electronic Structure and Third-Harmonic Generation in Asymmetric Double Inverse Parabolic Quantum Wells

Ozan ÖZTÜRK^{1,2*}

- ¹Department of Nanotechnology Engineering, Sivas Cumhuriyet University, 58140, Sivas, Türkiye
- ²Nanophotonics Application and Research Center, Sivas Cumhuriyet University, 58140, Sivas, Türkiye

Research Article

Article History:

Received: 07.02.2025 Accepted: 02.04.2025 Published online: 16.09.2025

Keywords:

Intense laser field Parabolic quantum well Third-harmonic generation

ABSTRACT

This study explores the effects of an intense laser field (ILF) on the energy levels, electron probability distributions, and third-harmonic generation (THG) coefficient in asymmetric double inverse parabolic quantum wells (ADIPQW). The Schrödinger equation is solved using the finite element method under the effective mass approximation, incorporating ILF effects via the Floquet method. For ILF parameter $\alpha_0 = 0, 2, 4, 6$, and 8 nm, we analyze the modifications in potential profiles, energy differences, dipole moment matrix elements (DMME), and THG coefficients. The results indicate that increasing ILF intensity leads to shifts in energy levels and electron localization. The energy differences E₂₁, E₃₁/2, and E₄₁/3 show distinct trends under varying ILF, directly affecting THG resonance peak positions. The DMME product remains nearly constant at low ILF values but fluctuates significantly at higher ILF intensities, peaking at $\alpha_0 = 5$ nm and reaching a minimum at $\alpha_0 = 7$ nm. These findings highlight ILF as a tunable parameter for controlling electronic properties and nonlinear optical responses in semiconductor quantum structures.

Asimetrik Çift Ters Parabolik Kuantum Kuyularındaki Yoğun Lazer Alanının Elektronik Yapı ve Üçüncü Harmonik Üretimi Üzerindeki Etkisi

Araştırma Makalesi

Makale Tarihcesi:

Geliş tarihi: 07.02.2025 Kabul tarihi:02.04.2025 Online Yayınlanma: 16.09.2025

Anahtar Kelimeler:

Yoğun lazer alanı Parabolik kuantum kuyusu Üçüncü harmonik üretimi

ÖZ

Bu çalısma, asimetrik çift ters parabolik kuantum kuyularında (ADIPOW) yoğun lazer alanının (ILF) enerji seviyeleri, elektron olasılık dağılımları ve üçüncü harmonik üretimi (THG) katsayısı üzerindeki etkilerini incelemektedir. Schrödinger denklemi, etkin kütle yaklaşımı çerçevesinde sonlu elemanlar yöntemi kullanılarak çözülmüş ve ILF etkileri Floquet yöntemi aracılığıyla modellenmiştir. ILF parametresi $\alpha_0 = 0, 2, 4, 6$ ve 8 nm için, potansiyel profillerindeki değişimler, enerji farkları, dipol moment matris elemanları (DMME) ve THG katsayıları analiz edilmiştir. Sonuçlar, ILF şiddetinin artmasının enerji seviyelerinde kaymalara ve elektron lokalizasyonunda değişimlere yol açtığını göstermektedir. Enerji farkları E21, E31/2, and E41/3, değişen ILF değerleri altında farklı eğilimler sergileyerek THG rezonans tepe noktalarını doğrudan etkilemektedir. DMME çarpanı düşük ILF değerlerinde neredeyse sabit kalırken, yüksek ILF şiddetlerinde önemli dalgalanmalar göstermekte, $\alpha_0 = 5$ nm'de maksimuma ulaşırken $\alpha_0 = 7$ nm'de minimum değerine inmektedir. Bu bulgular, ILF'nin yarı iletken kuantum yapılarında elektronik özellikleri ve doğrusal olmayan optik tepkileri kontrol etmek için ayarlanabilir bir parametre olarak işlev gördüğünü ortaya koymaktadır.

To Cite: Öztürk O. Influence of Intense Laser Field on the Electronic Structure and Third-Harmonic Generation in Asymmetric Double Inverse Parabolic Quantum Wells. Osmaniye Korkut Ata Üniversitesi Fen Bilimleri Enstitüsü Dergisi 2025; 8(4): 1644-1653

^{1,2}https://orcid.org/0000-0002-9592-3152

^{*}Corresponding author: ozanozturk@cumhuriyet.edu.tr

1. Introduction

The study of quantum well (QW) structures under external fields has attracted considerable attention due to their promising applications in optoelectronics and nonlinear optical devices. Among these external perturbations, intense laser fields (ILFs) stand out as a powerful tool for modifying the electronic and optical properties of low-dimensional semiconductor structures. Extensive research has been conducted on the interaction of ILFs with single and double quantum wells to explore their impact on energy levels, wave functions, and optical transition probabilities (Duque et al., 2011; Restrepo et al., 2015; Ozturk et al., 2019; Kasapoglu, 2024).

In particular, the influence of ILFs on symmetric and asymmetric quantum wells, such as GaAs/AlGaAs heterostructures, has been a subject of great interest. Studies have shown that ILFs alter the shape, depth, and width of potential wells, significantly affecting charge carrier localization and tunneling behavior (Ospina et al., 2015; Aktas et al., 2016). These modifications play a crucial role in determining transition energies and the optical response of semiconductor structures.

One of the key nonlinear optical phenomena investigated in laser-dressed quantum wells is third-harmonic generation (THG) coefficient. The THG coefficient is highly sensitive to external parameters, including ILF intensity and well geometry (Altuntas 2021; Sayrac et al., 2024). A previous study has reported that ILF-induced changes in energy spacing and dipole moment matrix elements (DMME) lead to noticeable shifts in THG resonance peaks (Alaydin et al., 2023). Furthermore, the ILF effect on THG coefficient in both single and double QW systems has been explored through various theoretical and computational methods, such as the effective mass approximation and density matrix formalism (Al et al., 2016; Tuzemen 2024). These investigations have provided valuable insights into the tunability of nonlinear optical responses, highlighting potential applications in photonic devices like frequency converters and optical modulators. In this study, we analyze the effects of ILFs on energy levels (ELs), electron probability distributions, DMMEs, and THG coefficients in an asymmetric double inverse parabolic quantum well (ADIPQW) structure. By systematically varying the ILF parameter, we examine the corresponding changes in the system's potential profile and electronic structure, particularly the shifts in THG resonance peaks. These findings are expected to contribute to the development of advanced optoelectronic and nonlinear optical devices.

2. Material and Methods

The Schrödinger equation for the GaAs/Al_xGa_{1-x} As QW structure is given in Eq. (1). To calculate the wave functions (WFs) and ELs under the effective mass approximation, we use the finite element method (Nakamura et al., 1989; Botero et al., 1992; Lepaul et al., 1996).

$$\left(-\frac{\hbar^2}{2m^*}\frac{d^2}{dz^2} + V(z)\right)\psi(z) = E\psi(z)$$
 (1)

The Hamiltonian includes a second-order differential equation, which is solved through diagonalization (Alaydin et al., 2022). The second derivative term is discretized as:

$$\frac{d^2}{dz^2} = \left[-2 \operatorname{diag}(\operatorname{ones}(1, N_z)) + \operatorname{diag}(\operatorname{ones}(1, N_z - 1), -1) + \operatorname{diag}(\operatorname{ones}(1, N_z - 1), 1) \right]^2$$
 (2)

Where the effective mass of the electron and the length of the matrix, and the confined potential are represented as m^* and N_z . V(z) is the potential seen along the z-direction by the electron, and E and $\Psi(z)$ are the eigen-energy and eigen-function related with the solution of Eq. (1), respectively.

$$V(z) = V_0 \begin{cases} -\frac{2}{L_L^2} \left(z + \frac{L_L + b}{2} \right)^2 & -\frac{L_L + b}{2} \le z \le -\frac{b}{2} \\ -\frac{2}{L_L^2} \left(z - \frac{L_R + b}{2} \right)^2 & \frac{b}{2} \le z \le \frac{L_R + b}{2} \\ 1 & \text{otherwise} \end{cases}$$
(3)

In this study, the left and right QW widths are $L_L=8$ nm and $L_R=12$ nm, the barrier width b=4 nm. Discontinuity on the side of the conduction band for this structure is analyzed using the following equation, $V_0=0.6~(1.155~x+0.37~x^2)~(eV)$; here 0.6 ratio is the conduction band-offset ratio and x symbolizes the contribution rate of Al in QWs. For x=0.3, the potential depth is $V_0=228$ meV. To solve Eq. (1), we take as base the eigenfunctions of the infinite potential well of width L(=60nm), which is given with $\phi_n(z)=\sqrt{\frac{2}{L}}\cos\left(\frac{n\,\pi\,z}{L}-\delta_n\right)$. Where $\delta_n=\begin{cases} 0 & n\text{ is old}\\ \pi/2 & n\text{ is even} \end{cases}$ and the wave function described the system is formed from a complete set as, $\Psi(z)=\sum_{n=1}c_n\,\phi_n(z)$, here c_n is the coefficient of the expansion.

To incorporate the effect of the non-resonant polarized ILF along the x-direction, the Floquet method is employed (Liu et al., 2022). In the high-frequency regime, a closed-form expression for the dressed potential is used. Consequently, the second term on the left-hand side of Eq. (1) is modified as $V(z) \rightarrow \langle V(z, \alpha_0) \rangle$ The laser-dressed confinement potential is then expressed as:

$$\langle V(z, \alpha_0) \rangle = \frac{\Omega}{2\pi} \int_0^{2\pi/\Omega} V(z + \alpha_0 \sin \Omega t) dt$$
 (4)

Here, $\alpha_0 = \sqrt{\frac{e^2 \, 8 \, \pi \, I_{laser}}{m^{*2} \, c \, \Omega^4}}$ is the laser-dressing parameter, e is the electron charge, I_{laser} is the mean intensity of the laser, Ω is the laser frequency and c is the light velocity (Yu et al., 2005; Karimi et al., 2015; Ozturk et al., 2022). After determining the wave functions (WFs) and energy levels (ELs), third-harmonic generation (THG) coefficients are calculated using the compact density matrix approach (Martínez-Orozco et al., 2012; Khordad, 2014; Ozturk et al., 2019; Zhang et al., 2022):

$$\chi_{3\omega}^{(3)} = \frac{e^4 \sigma_V}{\epsilon_0} \frac{M_{21} M_{32} M_{43} M_{41}}{(\hbar \omega - E_{21} - i\hbar \Gamma)(2\hbar \omega - E_{31} - i\hbar \Gamma/2)(3\hbar \omega - E_{41} - i\hbar \Gamma/3)} \tag{5}$$

The term M_{fi} represents the DMME and is defined as: $M_{fi} = \int \Psi_f^* \ z \ \Psi_i \ dz$, where ω is the angular frequency of the photon, ϵ_o is the vacuum permittivity, σ_v is the carrier density, $(E_{fi} = E_f - E_i = \hbar \ \omega_{fi})$, E_f and E_i are the final and initial energy states, respectively.

3. Results and Discussion

We have analyzed the THG coefficients in ADIPQW structure, both in the presence and absence of ILF. In this study, $m^* = 0.067 \text{ m}_0$ (m_0 is the free electron mass), $T = 1/\Gamma = 0.5 \text{ ps}$, $\sigma_v = 5 \text{x} 10^{22} \text{ m}^{-3}$.

For $\alpha_0 = 0, 2, 4, 6$, and 8 nm, Figure 1a–e illustrates the variation of the potential profile, consisting of an asymmetric double inverse parabolic, along with the probability distributions of electrons at each energy level. Under the influence of the ILF, the shape, depth and width of the potential wells determine the energy levels and the probability distributions of the electrons. For $\alpha_0 = 0$, electrons in the E₁ level are localized over a broader region in the right well, while those in the E2 level are confined to a narrower area in the left well. Electrons in the E3 and E4 levels are primarily found in the right and left wells, respectively, with slight tunneling into the adjacent wells. At $\alpha_0 = 2$ nm, the reduction in potential depth leads to an increase in energy levels. As the barrier width narrows, electrons in the E3 and E4 levels exhibit greater tunneling into other wells. At $\alpha_0 = 4$ nm, the shape of the inverse parabolic well on the left undergoes a complete transformation, eliminating the barrier between the E_3 and E_4 levels. Beyond $\alpha_0 = 4$ nm, the E_4 energy level decreases while the others rise. Electrons in E₁ become confined to a narrower well, whereas those in E₂ spread over a broader region. Meanwhile, electrons in the E₃ and E₄ levels extend across all well regions. When α_0 reaches 6 nm, the potential profile evolves into a structure consisting of three quantum wells (QWs). Electrons in the E₁ level are distributed across the two rightmost QWs, while those in higher energy levels spread throughout the entire region. At $\alpha_0 = 8$ nm, the potential now consists of four QWs. Electrons in E₁ localize within the three rightmost QWs, whereas electrons in the other levels remain distributed across all wells.

The energy differences (Figure 2a) and $|M_{21}M_{32}M_{43}M_{41}|$ product (Figure 2b) graphs are plotted at intervals of $\alpha_0 = 1$ nm. The inset illustrates the variation of |DMME| as a function of ILF parameter. As shown in Figure 2a, E_{21} energy difference remains nearly constant within the ranges of $0 \le \alpha_0 \le 2$ nm and $4 \text{ nm} \le \alpha_0 \le 6$ nm, while it increases for other α_0 values, reaching its maximum at α_0 =8 nm. The $E_{31}/2$ energy difference increases up to α_0 =3 nm and then remains constant for higher α_0 values.

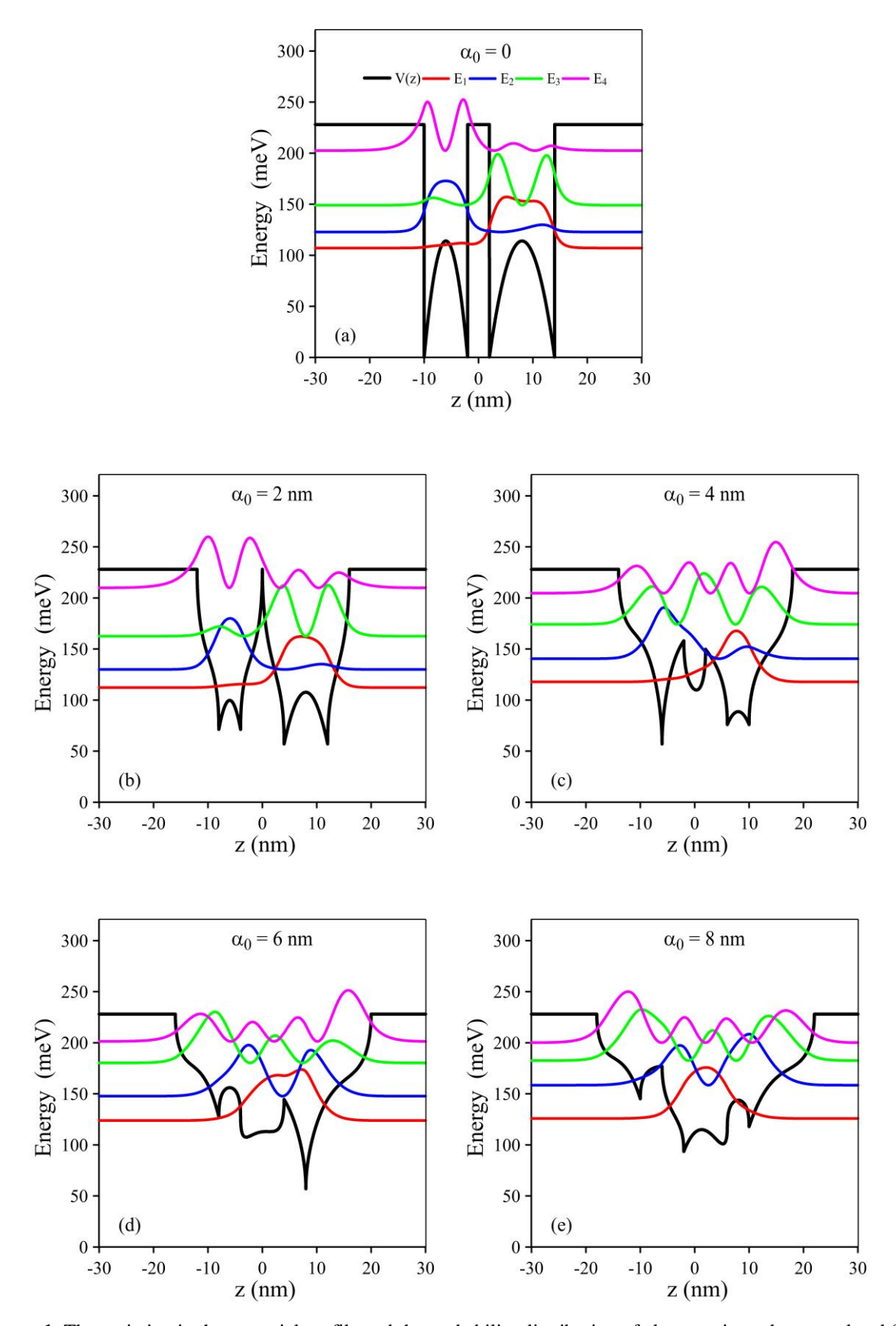


Figure 1. The variation in the potential profile and the probability distribution of electrons in each energy level for a) α_0 =0, b) α_0 =2 nm, c) α_0 =4 nm, d) α_0 =6 nm, e) α_0 =8 nm.

Meanwhile, $E_{41}/3$ stays nearly constant up to $\alpha_0=2$ nm but decreases as α_0 increases further. The $|M_{21}M_{32}M_{43}M_{41}|$ product remains constant for $0 \le \alpha_0 \le 1$ nm, starts increasing after $\alpha_0=2$ nm, reaches a maximum at $\alpha_0=5$ nm, and a minimum at $\alpha_0=7$ nm. This minimum value is due to the $|M_{41}|$ DMME value being very small (0.032 nm) at $\alpha_0=7$ nm. For $\alpha_0=0$, the values of $|M_{21}|$, $|M_{32}|$ and $|M_{43}|$ are almost the same, while $|M_{41}|$ has a significantly lower value. As the ILF parameter increases, the upper regions of the potential profile expand, leading to an increase in $|M_{43}|$ and $|M_{32}|$ due to the overlap of wave functions in these regions. The $|M_{21}|$ value exhibits a small peak at $\alpha_0=6$ nm, which can be attributed to the fact that, at this ILF value, electrons in the E_1 energy level have a higher probability of being distributed over a wider region and overlapping with the wave function of electrons in the E_2 energy level. On the other hand, due to the minimal overlap between the wave functions of electrons in the E_1 and E_4 energy levels, the $|M_{41}|$ value remains quite low.

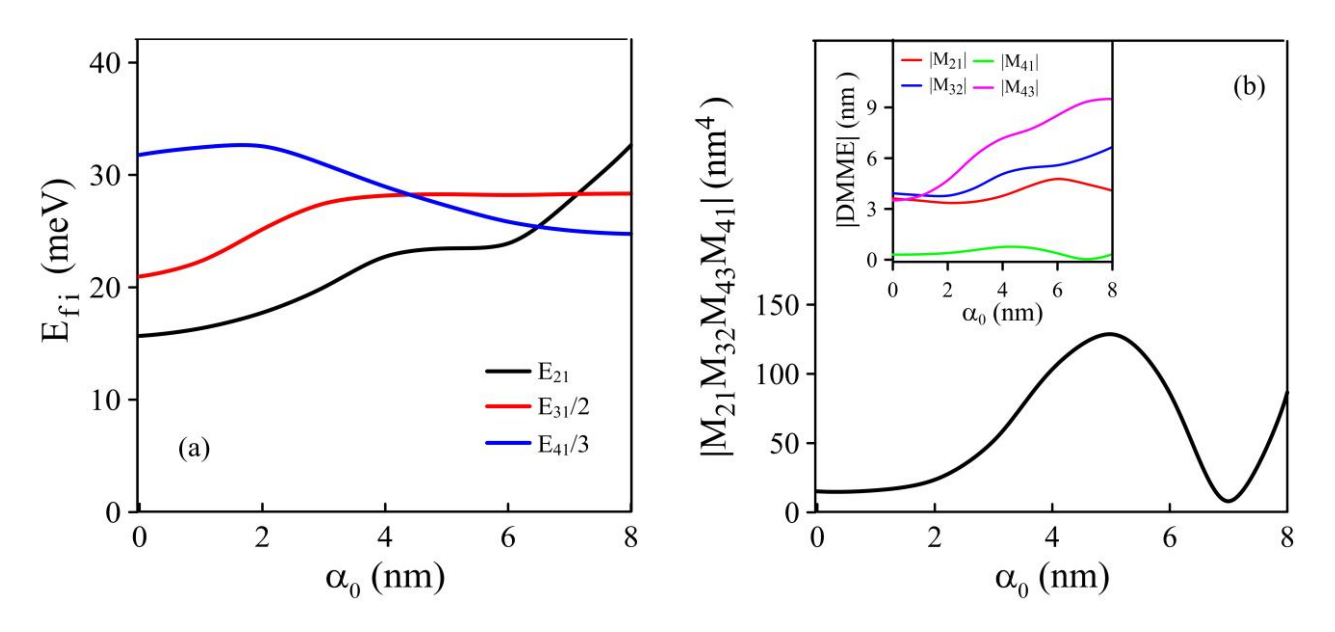


Figure 2. a) Energy differences and b) $|M_{21}M_{32}M_{43}M_{41}|$ product as a function of the ILF parameter. The inset illustrates the variation of |DMME|| versus ILF.

Figure 3 displays THG coefficients for different ILFs, with coefficients for α_0 of 0 and 2 nm scaled by 20. For the THG coefficient case, the resonance peaks are positioned at $E_{41}/3 \approx \hbar\omega$ (major peak), $E_{31}/2 \approx \hbar\omega$ (middle peak), and at $E_{21} \approx \hbar\omega$ (minor peak). Minor peaks associated with E_{21} and middle peaks related to $E_{31}/2$ exhibit blue shifts, while the maximum peaks corresponding to $E_{41}/3$ show red shifts. For different ILF values, transition energies are provided in Table 1. Both the $E_{21}-E_{31}/2$ and $E_{21}-E_{41}/3$ energy differences are negative for $0 \leq \alpha_0 \leq 6$ nm but positive only at α_0 =8 nm. This implies that for α_0 =8 nm, the minor peak in the THG coefficient graph appears at a higher photon energy scale, positioned further to the right. The $E_{31}/2-E_{41}/3$ difference is negative for $0 \leq \alpha_0 \leq 4$ nm and becomes positive afterward. This means that for α_0 =6 nm and 8 nm, the middle peak of the THG coefficient should be located to the right of the maximum peak. The inset of the THG coefficient displays the curves for $\alpha_0 = 0$ and 2 nm,

showing their actual values. As shown in Table 1, in both cases, the minor peak appears on the far left, while the maximum peak is on the far right. For α_0 =0, since the E_{21} energy difference is close to the $E_{31}/2$ energy difference, the middle peak appears larger than the maximum peak. For α_0 =4 nm, the DMME product is large, and since the $E_{31}/2$ and $E_{41}/3$ energy differences are close to each other, the THG coefficient is significantly high. At α_0 =6 nm, the middle peak is to the right, the maximum peak is to the left, and the E_{21} and $E_{41}/3$ values are close to each other. For α_0 =8 nm, from left to right, the maximum, middle, and minor peaks are observed. The positions of the maximum, middle, and minimum peaks of the THG coefficient are also consistent with Fig. 2a and Table 1.

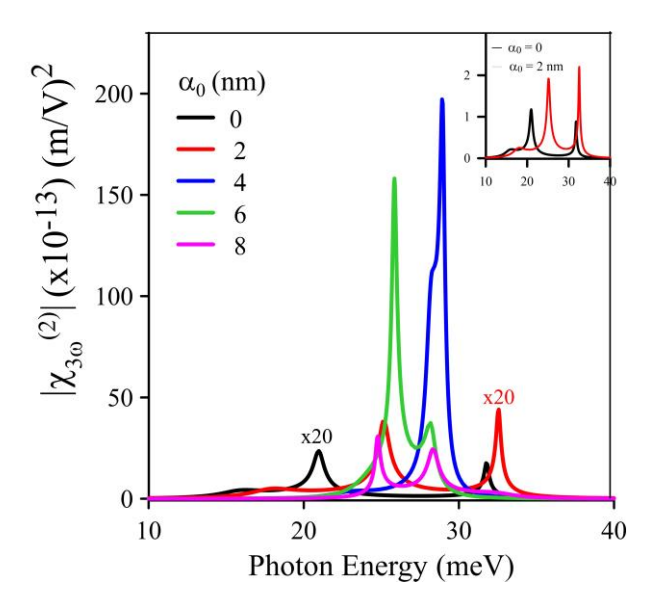


Figure 3. THG coefficients with varying ILF. At $\alpha_0 = 0$ nm and 2 nm, the THG coefficients are multiplied by 20. In the inset of the THG coefficient, the curves for α_0 =0 and 2nm are presented with their actual values.

-7.42

-5.43

-4.30

4.31

Table 1. Transition energies for different ILF values.

-7.39

-0.79

2.37

3.58

-14.81

-6.23

-1.93

7.89

4. Conclusion

2

4

6

In this study, we investigated the impact of ILF on the energy differences, electron probability distributions, DMMEs, and THG coefficients in ADIPQW. The results demonstrate that ILF significantly alters the potential profile, leading to energy shifts and modifications in electron localization. At low ILF values, electrons remain confined within specific wells, whereas at higher ILF intensities, potential barriers are suppressed, facilitating tunneling and delocalization. THG coefficient analysis reveals that resonance peak positions shift with ILF intensity. Minor and middle peaks associated with E_{21} and $E_{31}/2$ experience blue

shifts, whereas maximum peaks linked to E₄₁/3 exhibit red shifts. The variation in DMME values with ILF further influences the intensity of THG coefficients. These findings underscore the potential of ILF as a precise tuning mechanism for quantum well electronic structures and nonlinear optical properties. Future studies may extend this analysis to different quantum well geometries and materials, further optimizing ILF-controlled optoelectronic applications.

Conflict of Interest Statement

The author of the article declares that there is no conflict of interest.

Summary of Researchers' Contribution Declaration

The author declares that he contributed 100% of the article.

References

- Aktas S., Kes H., Boz FK., Okan SE. Control of a resonant tunneling structure by intense laser fields. Superlattices and Microstructures 2016; 98: 220-227.
- Al EB., Yeşilgül Ü., Ungan F., Kasapoğlu E. Nonlinear optical rectification, the second and third harmonic generation in asymmetric double quantum well under the intense laser field. Cumhuriyet Üniversitesi Fen Edebiyat Fakültesi Fen Bilimleri Dergisi 2016; 37(4): 405-411.
- Alaydin BO., Altun D., Ozturk E. Linear and nonlinear optical properties of semi-elliptical InAs quantum dots: Effects of wetting layer thickness and electric field. Thin Solid Films 2022; 755: 139322.
- Alaydin BO., Altun D., Ozturk O., Ozturk E. High harmonic generations triggered by the intense laser field in GaAs/Al_xGa_{1-x}As honeycomb quantum well wires. Materials Today Physics 2023; 38: 101232.
- Altuntas I. Effects of applied external fields on the nonlinear optical rectification, second, and third harmonic generation in a quantum well with exponentially confinement potential. The European Physical Journal B 2021; 94(9): 177.
- Botero J., Shertzer J. Direct numerical solution of the Schrodinger equation for quantum scattering problems. Physical Review A 1992; 46(3): R1155-R1158.
- Duque CA., Mora-Ramos ME., Kasapoglu E., Sari H., Sökmen I. Intense laser field effect on impurity states in a semiconductor quantum well: transition from the single to double quantum well potential. The European Physical Journal B 2011; 81(4): 441-449.
- Karimi MJ., Vafaei H. Second-order nonlinear optical properties in a strained InGaN/AlGaN quantum well under the intense laser field. Superlattices and Microstructures 2015; 78: 1-11.
- Kasapoglu E. Non-resonant intense laser field and electric field effects on the optical characterization of Rosen-Morse quantum wells with different potential functions. Optical and Quantum Electronics 2024; 56(9): 1425.
- Khordad R. Second and third-harmonic generation of parallelogram quantum wires: electric field. Indian Journal of Physics 2014; 88(3): 275-281.

- Lepaul S., Lustrac AD., Bouillault F. Solving the Poisson's and Schrodinger's equations to calculate the electron states in quantum nanostructures using the finite element method. IEEE Transactions on Magnetics 1996; 32(3): 1018-1021.
- Liu G., Cao Y., Liu R., Chen G., Wu F., Zheng Y., Chen Z., Guo K., Lu L. Terahertz laser field manipulation on the electronic and nonlinear optical properties of laterally-coupled quantum well wires. Optics Express 2022; 30(4): 5200-5212.
- Martínez-Orozco JC., Mora-Ramos ME., Duque CA. Nonlinear optical rectification and second and third harmonic generation in GaAs δ-FET systems under hydrostatic pressure. Journal of Luminescence 2012; 132(2): 449-456.
- Nakamura K., Shimizu A., Koshiba M., Hayata K. Finite-element analysis of quantum wells of arbitrary semiconductors with arbitrary potential profiles. IEEE Journal of Quantum Electronics 1989; 25(5): 889-895.
- Ospina DA., Akimov V., Mora-Ramos ME., Morales AL., Tulupenko V., Duque CA. Optical properties of a multibarrier structure under intense laser fields. Superlattices and Microstructures 2015; 87: 109-114.
- Ozturk O., Alaydin BO., Altun D., Ozturk E. Intense laser field effect on the nonlinear optical properties of triple quantum wells consisting of parabolic and inverse-parabolic quantum wells. Laser Physics 2022; 32(3): 035404.
- Ozturk O., Ozturk E., Elagoz S. The effect of intense laser field on the nonlinear optical features in asymmetric multiple step and inverse V-shaped multiple step quantum wells. Laser Physics 2019; 29(10): 105401.
- Ozturk O., Ozturk E., Elagoz S. Nonlinear optical rectification, second and third harmonic generations in square-step and graded-step quantum wells under intense laser field. Chinese Physics Letters 2019; 36(6): 067801.
- Restrepo RL., Morales AL., Akimov V., Tulupenko V., Kasapoglu E., Ungan F., Duque CA. Intense laser field effects on a Woods–Saxon potential quantum well. Superlattices and Microstructures 2015; 87: 143-148.
- Sayrac M., Dakhlaoui H., Belhadj W., Ungan F. Effect of structural parameters and applied external fields on the third harmonic generation coefficient of AlGaAs/GaAs three-step quantum well. The European Physical Journal Plus 2024; 139(1): 57.
- Tuzemen AT. Effects of external fields and structural parameters on third harmonic generation of GaAs/AlGaAs Manning-like double quantum well structure. The European Physical Journal Plus 2024; 139(6): 513.
- Yu YB., Zhu SN., Guo KX. Exciton effects on the nonlinear optical rectification in one-dimensional quantum dots. Physics Letters A 2005; 335(2): 175-181.

Zhang ZH., Yuan JH. The nonlinear second harmonic generation and third harmonic generation in GaAs/GaAlAs exponentially confined quantum well: Electric and magnetic field effects. Physica B: Condensed Matter 2022; 646: 414356.